Folding events in the 21–30 region of amyloid β-protein (Aβ) studied *in silico*

Jose M. Borreguero*†, Brigita Urbanc*, Noel D. Lazo‡, Sergey V. Buldyrev§, David B. Teplow‡, and H. Eugene Stanley*

*Center for Polymer Studies and Department of Physics, Boston University, Boston, MA 02215; ‡Department of Neurology, David Geffen School of Medicine, University of California, Los Angeles, CA 90095; and §Department of Physics, Yeshiva University, New York, NY 10033

Oligomeric assemblies of the amyloid β-protein (Aβ) have been implicated in the pathogenesis of Alzheimer's disease as a primary source of neurotoxicity. Recent *in vitro* studies have suggested that a 10-residue segment, Ala-21–Ala-30, forms a turn-like structure that nucleates the folding of the full-length Aβ. To gain a mechanistic insight, we simulated Aβ(21–30) folding by using a discrete molecular dynamics algorithm and a united-atom model incorporating implicit solvent and a variable electrostatic interaction strength (EIS). We found that Aβ(21–30) folds into a loop-like conformation driven by an effective hydrophobic attraction between Val-24 and the butyl portion of the Lys-28 side chain. At medium EIS [1.5 kcal/mol (1 cal = 4.18 J)], unfolded conformations almost disappear, in agreement with experimental observations. Under optimal conditions for folding, Glu-22 and Asp-23 form transient electrostatic interactions (EI) with Lys-28 that stabilize the loop conformations. Glu-22–Lys-28 is the most favored interaction. High EIS, as it occurs in the interior of proteins and aggregates, destabilizes the packing of Val-24 and Lys-28. Analysis of the unpacked structures reveals strong EI with predominance of the Asp-23–Lys-28 interaction, in agreement with studies of molecular modeling of full-length Aβ fibrils. The binary nature of the EI involving Lys-28 provides a mechanistic explanation for the linkage of amino acid substitutions at Glu-22 with Alzheimer's disease and cerebral amyloid angiopathy. Substitutions may alter the frequency of Glu-22 or Asp-23 involvement in contact formation and affect the stability of the folding nucleus formed in the Aβ(21–30) region.

molecular dynamics | Alzheimer's disease | nucleation | protein folding

Alzheimer's disease (AD) is a neurodegenerative disorder characterized pathologically by the extracellular deposition of amyloid fibrils and the intracellular formation of neurofibrillary tangles. Amyloid fibrils are composed of the amyloid β-protein (Aβ), which exists predominantly *in vivo* as a 40- or 42-residue protein produced by cleavage from the Aβ precursor. Amyloid fibrils were shown to be neurotoxic (1), but subsequent biophysical, biological, and clinical data indicated that smaller assemblies also were neurotoxic (2–4). More recent studies addressed the toxicity of soluble oligomeric Aβ assemblies (5–9). Taken together, these data suggest that small oligomers, not fibrils, may be the proximate toxin that causes neurodegeneration. An attractive strategy for drug development suggests itself: Prevent the formation of toxic oligomers. To do so, knowledge of the structure and dynamics of Aβ monomer under conditions that favor oligomerization is necessary.

Recent limited proteolysis experiments on Aβ(1–40) and Aβ(1–42) identified protease-resistant segments under conditions favoring oligomerization (10). A 10-residue segment, Ala-21–Ala-30, was highly resistant to proteolytic attack, indicating the presence of a folded structure. Lazo *et al.* (10) postulated that this structure nucleates the intramolecular folding of Aβ monomer. Notably, the homologous decapeptide Aβ(21–30) showed similar protease resistance when studied in monomeric solution, lending support to the hypothesis. Determination of the solution structure of Aβ(21–30) by NMR yielded two families of structures containing a turn-like motif centered at residues Gly-25–Ser-26. Putative stabilization factors are (*i*) intrinsic turn propensities of Gly-25, Ser-25, and Asn-27; (*ii*) hydrophobic interaction between Val-24 and the butyl portion of the Lys-28 side chain; and (*iii*) electrostatic interactions (EI) between Glu-22 and Lys-28 or between Asp-23 and Lys-28. These latter interactions defined the two families and led to the question, Which of the two families of structures is preferred? Lazo *et al.* also postulated that partial unfolding of the Ala-21–Ala-30 region may be necessary for the subsequent fibrillization of Aβ. How might this unfolding occur?

To address these questions, we used an *in silico* approach to visualize the folding/unfolding of Aβ(21–30). Computer simulations, particularly molecular dynamics (MD) simulations, can provide information that cannot be obtained by experimental methods, including conformational transitions that occur at every step along the folding/unfolding pathway. MD simulations also can contribute to a better understanding of the forces (e.g., electrostatic versus hydrophobic) controlling protein folding. Discrete MD (DMD) combined with a coarse-grain protein model has been used to study protein folding (11–13) and aggregation (14–17, 22). We present here results of studies of the conformational dynamics of Aβ(21–30) folding obtained by using DMD simulations in conjunction with a united-atom model and implicit solvent. The results agree with NMR-determined structures for monomeric Aβ(21–30) in aqueous solution, provide a theoretical basis for understanding the pathologic effects of mutations at position 22, and suggest that our model will be useful for *in silico* testing of mechanistic hypotheses about Aβ folding and its therapeutic control.

Methods

Protein Model. Our united-atom model, which is an extension of a recently used DMD model (18), represents all protein atoms except hydrogen. Of relevance to our study are the atomic interactions implemented, namely (*i*) backbone hydrogen bonds, (*ii*) effective interactions mimicking EI between charged atoms of the side chains, and (*iii*) implicit solvent effects mediated by hydropathic interactions between side chain atoms.

MD. We performed DMD simulations and monitored the time evolution of Aβ(21–30) trajectories. We simulated the conformational changes of Aβ(21–30) for 10^6 time units ($\cong 50$ ns with the selected energy scale). This time span is much smaller than typical folding times of isolated hairpins in solution (19). However, we can effectively sample the conformational space of Aβ(21–30) because of our implicit treatment of solvent and hydrogen atoms, thus increasing the conformational freedom of the peptide and reducing the complexity of the energy landscape (20). We simulated Aβ(21–30) folding at six different EI

BIOPHYSICS

Table 1. 1-loop and 2-loop radii for amino acids of the distal hairpin of the c-Crk Src homology 3 (SH3) domain

	c-Crk SH3(173–178)	
	1-loop, r1	2-loop, r2
$i - 1$	5.9	30.0
i	6.4	13.0
$i + 1$	3.9	5.0
$i + 2$	3.9	4.4
$i + 3$	4.0	7.5
$i + 4$	5.1	17.0

Table 2. 1-loop and 2-loop radii for amino acids of the distal hairpin of the Aβ(21–30)

	Aβ(21–30)	
	1-loop, $r1 \pm \sigma(r1)$	2-loop, $r1 \pm (r2)$
Glu-22	6.1 ± 0.9	—
Asp-23	5.1 ± 1.0	8.6 ± 4.3
Val-24	4.7 ± 0.9	10.2 ± 8.7
Gly-25	6.0 ± 1.6	13.4 ± 14.4
Ser-26	6.3 ± 0.9	8.3 ± 2.5
Asn-27	5.1 ± 1.1	8.3 ± 4.4
Lys-28	5.2 ± 1.2	10.9 ± 5.2
Gly-29	5.6 ± 1.6	—

Data are shown as mean ± SD. Standard error of the average equals the SD divided by $\sqrt{N_{idp}} \approx 7.9$.

strengths (EIS) in the range of 0.00–2.50 kcal/mol (1 cal = 4.18 J) and recorded $N = 2,000$ conformations for each trajectory.

Structural Determinants. We characterized the structures that Aβ(21–30) adopts in the course of the simulation by computing (*i*) the propensity of each amino acid to be at the center of a loop (see below); (*ii*) the combined solvent-accessible surface area (SASA) (21) of the Val-24 and Lys-28 side chains, which assumes a much smaller area in the Aβ(21–30) loop conformation centered at Ser-26 than in a random coil or in a loop conformation centered at a residue other than Ser-26; (*iii*) average distances and deviations between all pairs of C^α atoms; and (*iv*) the α angle, defined as the angle between the vector $\vec{v}$ joining C^α and N^ζ atoms of Lys-28 and the plane generated by the C^α atoms of Val-24, Ser-26, and Lys-28. α is positive if the projection of $\vec{v}$ onto the normal vector to the loop–plane, $\vec{n}$, is positive (Fig. 2*b Inset*). The Lys-28 side chain points above the plane for positive α and below the plane for negative α.

We defined the k-loop radius for amino acid i as the radius of the circle passing through the C^α atoms of amino acids $(i - k)$, i, and $(i + k)$. We computed for each amino acid the 1-loop ($k = 1$) and the 2-loop ($k = 2$) radii during the simulation span and obtained the histograms of 1- and 2-loop radii. The 1-loop radius depends only on the local (Φ and Ψ) angles. Small 1-loop values indicate a preference for a local sharp bend or a part of a turn, and large values indicate a preference for locally extended conformations. Small 2-loop values indicate a preference of the amino acid to be at the center of a loop comprising five amino acids, which could be classified either as a turn or as an unstructured loop.

We computed 1-loop and 2-loop radii for the distal hairpin of c-Crk Src homology 3 domain protein (residues 173–178), which we take as a model hairpin (Table 1). Residues in the turn are labeled as i, $(i + 1)$, $(i + 2)$, and $(i + 3)$. Residues $(i + 1)$ and $(i + 2)$ show the lowest 1-loop and 2-loop radii and serve as a reference for our results with the Aβ(21–30) simulations (Table 2).

Results

In preliminary studies of Aβ(21–30), we used a simplified, four-bead model with amino acid-specific hydropathic interactions (17) and effective EI. Aβ(21–30) folding studied with this model indicated a bend in the Gly-25–Asn-27 region only under strong EI ($\cong 4$ kcal/mol) (data not shown). However, it is not clear if and how such a strong EI can occur when charged amino acids are exposed to the solvent. A more sophisticated model was needed to test the nature of Aβ(21–30) folding at the atomic level; therefore, we adopted the united-atom model with implicit solvent.

Relaxation Time. Fluctuations of the potential energy at equilibrium conditions take ≈16×10^3 computer time steps to relax. During this time span, we recorded ≈32 conformations. Thus, the number of statistically independent measurements in our simulation, N_{idp}, is the total number of measurements, N ($N = 2,000$), divided by the number of consecutive correlated measurements, $N_{idp} = N/32 \cong 62$ (23).

1-Loop and 2-Loop Radii. We first simulated Aβ(21–30) dynamics without the hydropathic and electrostatic components of the force field. Under these conditions, Val-24 and Ser-26 have the smallest and biggest average 1-loop radii, respectively, and both values are bigger than the typical 1-loop radii of a β-turn (see *Methods* and Table 2). The peptide tends to bend in the immediate vicinity of Val-24 and tends to adopt more locally extended conformation around Ser-26. Gly-25 and Gly-29 have the biggest standard deviations of 1-loop radii, reflecting the wider range of allowed Φ and Ψ values for Gly. Regarding the average 2-loop radii (Table 2), Ser-26 and Asn-27 display the two smallest values. The emerging picture for the preferred peptide conformation under no hydropathy and electrostatics interactions is a broad loop with the center at Ser-26 and Asn-27. The loop is broad because of the large 1-loop radius for Ser-26.

SASA. Under conditions of no hydropathy and irrespective of the EIS, the SASA distribution shows a single peak corresponding to the sum of the separate SASA values for solvent-exposed Val-24 and Lys-28 (≈350 Å) (Fig. 1*a*, peak A). "Switching on" hydropathic interactions results in an additional peak with a smaller SASA (≈245 Å, a 30% decrease) (Fig. 1*b*, peak B). We denote the set of conformations with SASA values within peak B as conformations of class *B*. For these conformations, Aβ(21–30) adopts a loop conformation centered at Ser-26 and the Val-24 propyl side chain packs against the butyl portion of the Lys-28 side chain because of an effective hydrophobic attraction. EI modulate the population of the peaks but does not shift the average SASA values (Table 3). Thus, EI affect the probability that the loop will form but do not alter the way in which Val-24 and Lys-28 pack against each other once the loop has formed. The Val-24–Lys-28 packing probability increases when we increase the EIS from 0 to 1.5 kcal/mol and then decreases upon a further EIS increase. Analysis of the unpacked conformations at a high EIS reveals the formation of contacts Glu-22–Lys-28 (23% of the cases), Asp-23–Lys-28 (48% of the cases), or both (29% of the cases). These interactions inhibit the ability of Val-24 and Lys-28 to pack against each other.

C^α–C^α Distances and σ Values. The C^α–C^α distance between Val-24 and Lys-28 when in a loop conformation (5.3 ± 0.5 Å) is 32% smaller than the distance in the absence of hydropathy and EI (7.8 ± 1.3 Å) (Fig. 1*c*). Once the loop forms, the EIS has no apparent effect on the C^α–C^α distance, indicating again that electrostatics does not alter the way in which Val-24 and Lys-28 pack against each other. Contacts involving either Val-24 or
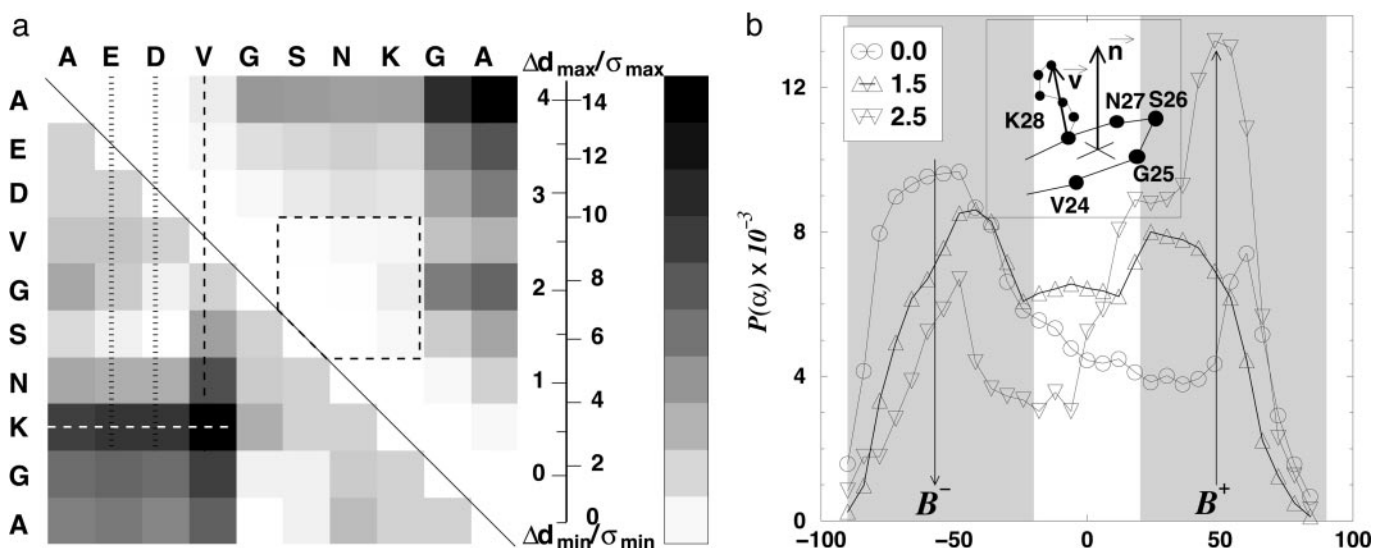
Fig. 1. Val-24–Lys-28 packing. (*a*) Distributions of SASA with a variable EIS and with no hydropathic interactions. (*b*) Same probability distributions as in *a*, but hydropathic interactions are present. (*c*) Val-24–Lys-28 C^α–C^α distance distributions under the conditions of *a*. (*d*) Same distance distributions as in *c*, but hydropathic interactions are present.

Lys-28 show the largest distance reduction upon loop formation, emphasizing the role of electrostatic and hydrophobic interactions in the stabilization of the loop.

We estimate the loop flexibility with the standard deviation σ of the C^α–C^α distance (Fig. 2*a*). The error of a σ value is the σ value itself divided by $\sqrt{N_{idp}}$, $\approx 13\%$ of the value. Contacts Ala-21–Ser-26 and Ser-26–Ala-30 have high σ values, indicating that the two sides of the loop [$A\beta$(21–26) and $A\beta$(26–30), respectively] are more flexible than analogous sides of a putative β-hairpin conformation. Interside C^α–C^α distances for termini contacts Glu-22–Ala-30 (12.6 Å) and Asp-23–Gly-29 (11.1 Å) indicate rare contact formation. C^α–C^α distances for Val-24–Lys-28 (6.4 Å) and Gly-25–Asn-27 (6.7 Å) are small enough to be associated with loops but large enough to prevent the formation of any stable hydrogen bond in the backbone. In summary, the loop has no stable hydrogen bonds in the backbone, is stable in the region Val-24–Lys-28, and fluctuates at the termini.

α Angle. Regardless of the EIS, class *B* conformations present a bimodal distribution of α values, with broad peaks at negative and positive α values. (Fig. 2*b*). We denote the set of conformations within class *B* with $-90° < \alpha < -20°$ as conformations of class B^-. These loop conformations feature Lys-28 pointing below the loop plane. Analogously, we construct class B^+ with class *B* conformations with $20° < \alpha < 90°$. The population of class B^- (B^+) decreases (increases) with increasing EIS (Fig. 2*b*).

Table 3. Percent probability of observing class *B* conformations

EI, kcal/mol	B	B⁻	B⁺
0.00	74	40	20
1.50	97	38	34
2.50	80	20	44

Shown are the percent probabilities of a class *B* conformation (loop), class B^- (Lys-28 pointing below the loop plane), and class B^+ (Lys-28 pointing above).

and Table 3). We observe that the Glu-22–Lys-28 contact is three to five times more likely to form (the particular value depending on the applied EIS) if Lys-28 is pointing above the plane (see Table 4). In contrast, the Asp-23–Lys-28 interaction shows no preference with Lys-28 orientation. Thus, Glu-22 controls the population of the peaks in the α angle distribution. At optimal EI for loop stability (≈ 1.5 kcal/mol), we observe that Glu-22 has a higher propensity to interact with Lys-28 than does Asp-23.

Discussion

Recent NMR studies of $A\beta$(25–35) (24) show a type I β-turn centered at amino acids Ser-26 and Asn-27. Molecular modeling of fibrils formed by $A\beta$(1–40) (25), $A\beta$(12–42) (26), and $A\beta$(16–35) (27) predicts a turn or bend in the region Gly-25–Lys-28. In fact, this region has an intrinsic propensity to form a type I or type VII turn (28). Consistent with these results, we observe that Ser-26 and Asn-27 have a higher propensity to be at the center of a loop than any other of the amino acids in our $A\beta$(21–30) model when simulated in the absence of hydropathic interactions and EI.

Addition of hydropathic interactions induces a semistable loop conformation in $A\beta$(21–30), with the center at Ser-26. Hydrophobic interactions are critical for the stabilization of isolated β-hairpins (29). Espinosa *et al.* (30) pointed out the correlation between hairpin stability and the distance of the hydrophobic amino acids to the turn, with smaller distances leading to greater stability. We observe that Val-24 and Lys-28, two amino acids in the proximity of Ser-26, pack against each other because of the hydrophobic effect. The SASA reduction associated with Val-24–Lys-28 packing is relatively small compared with the typical SASA reduction in hairpins stabilized by the hydrophobic interaction (29), which may explain the inability of $A\beta$(21–30) to stabilize in a hairpin conformation during the course of our simulations.

The observed absence of backbone hydrogen bonds agrees with ¹H NMR and the hydrogen exchange experiments of Lazo *et al.* (10). We argue from our results that $A\beta$(21–30) adopts a semirigid loop in the Val-24–Lys-28 region, whereas the termini

BIOPHYSICS

Fig. 2. Geometric characterizations of folded Aβ (21–30) conformations. (*a*) The upper-right triangle shows the standard deviation, σ, of the C^{α}–C^{α} distance ($\sigma_{min} \equiv 0.0$ Å $< \sigma < \sigma_{max} \equiv 13.8$ Å) for loop conformations. Contacts within the square have minimal σ values and correspond to loop contacts. The lower-right triangle shows the average distance reduction in the C^{α}–C^{α} distance when Aβ(21–30) adopts a loop conformation, ($\Delta d_{min} \equiv 3.8$ Å $< \Delta d < \Delta d_{max} \equiv 14.9$ Å). (*b*) α angle distributions for different EIS are all bimodal. The heights of the peaks follow the arrows with increasing EIS. (*Inset*) Vectors $\vec{v}$ and $\vec{n}$ for a loop conformation.

are highly flexible. Similar conclusions were made by Hou *et al.* (31) based on NMR experiments of Aβ(1–40) and Aβ(1–42). The finding that Lys-28 flips its orientation during the simulation is a direct consequence of the flexibility of the termini. In a hairpin configuration, a flip in the orientation of Lys-28 would require breaking three backbone hydrogen bonds, an energetically unfavorable process.

Under optimal conditions for loop stability (EI ≈ 1.5 kcal/mol), Lys-28 shows no preference to point above or below the loop plane. Lys-28 preferentially points above the loop plane at a high EIS because the bias of the Glu-22–Lys-28 interaction with Lys-28 orientation becomes prominent under these conditions. The bias is in agreement with structure calculations by Lazo *et al.* (10), who observed a Coulombic interaction between Glu-22 and Lys-28 for the model structure in which Lys-28 is pointing above the loop plane. In the structural model of Aβ(1–40) fibrils proposed by Petkova *et al.* (25), Lys-28 points above the loop plane and forms a salt bridge with Asp-23. Our results suggest that Glu-22 would inhibit formation of this salt bridge because Lys-28 preferentially interacts with Glu-22 when pointing above the plane.

EI affect loop stability differently than do hydropathic interactions. Whereas hydropathic effects are "bulky" in nature (for instance, the whole side chain of Val-24 interacting with the butyl portion of Lys-28), EI are selective because they involve only two charged atoms. Thus, we expected that EI might modulate, but not determine, the conformational dynamics of Aβ(21–30). EI stabilize the loop conformations in the range of EIS typical of interacting charged residues at the surface of proteins (32, 33)

(0.0–1.5 kcal/mol). Thus, we argue that EI and hydropathic interactions cooperate to maximize the stability of loop conformations when Aβ(21–30) is solvent-exposed. Glu-22 is more likely to interact with Lys-28 than is Asp-23 (Table 4) and, thus, may be more prominent in stabilizing the Aβ(21–30) monomer fold.

In contrast, EI destabilize the loop conformations in the range of the EIS of interacting charged residues in the interior of proteins and aggregates (EI > 1.5 kcal/mol) (34). Asp-23 is more likely to interact with Lys-28 than is Glu-22, inhibiting the ability of Lys-28 to pack against Val-24 (Fig. 3*a*). Thus, we hypothesize that before fibril formation, the region Aβ(21–30) partially unfolds, disrupting the Val-24–Lys-28 contact. The observed prevalence of the Asp-23–Lys-28 interaction is in agreement with molecular models of fibrils formed by full-length Aβ(25) and Aβ(16–35) (27), which show stabilization through Asp-23–Lys-28 interactions and no Glu-22–Lys-28 interaction or Val-24–Lys-28 packing. In recent kinetics experiments, Sciarretta *et al.* (35) observed an increase of three orders of magnitude of fibrillogenesis upon stabilization of the Asp-23–Lys-28 interaction by means of an engineered lactam bridge. This observation led the authors to suggest that stabilization of the salt bridge Asp-23–Lys-28 in the core of the fibril may be the rate-limiting step in the process of fibril formation. A hypothesis that may explain this observation is a desolvation barrier upon burial of Asp-23 inside the core of the protofibril. This hypothesis rationalizes the observed increase in the rate of fibril formation (36) associated to the familial AD mutation Asp-23-Asn (Iowa mutation). The desolvation barrier for Asn may be lower than that for Asp, and Asn-23 still can form a stable hydrogen bond with Lys-28 in the core of the fibril.

Increases in the rate of fibril growth also are observed in peptides with amino acid substitutions linked to other familial AD mutations, including Glu-22-Gly (Arctic), Glu-22-Gln (Dutch), and Glu-22-Lys (Italian). However, the desolvation hypothesis barrier does not hold when applied to Glu-22, because Glu-22 is solvated in the model fibril (25). Our results suggest a different mechanism for the "protective" role of Glu-22. If fibril formation requires a rearrangement of the Aβ(21–30) region involving denaturation of the Val-24–Lys-28

Table 4. Percent probability of forming Glu-22–Lys-28 and Asp-23–Lys-28 contacts for conformations of class B, B^-, and B^+

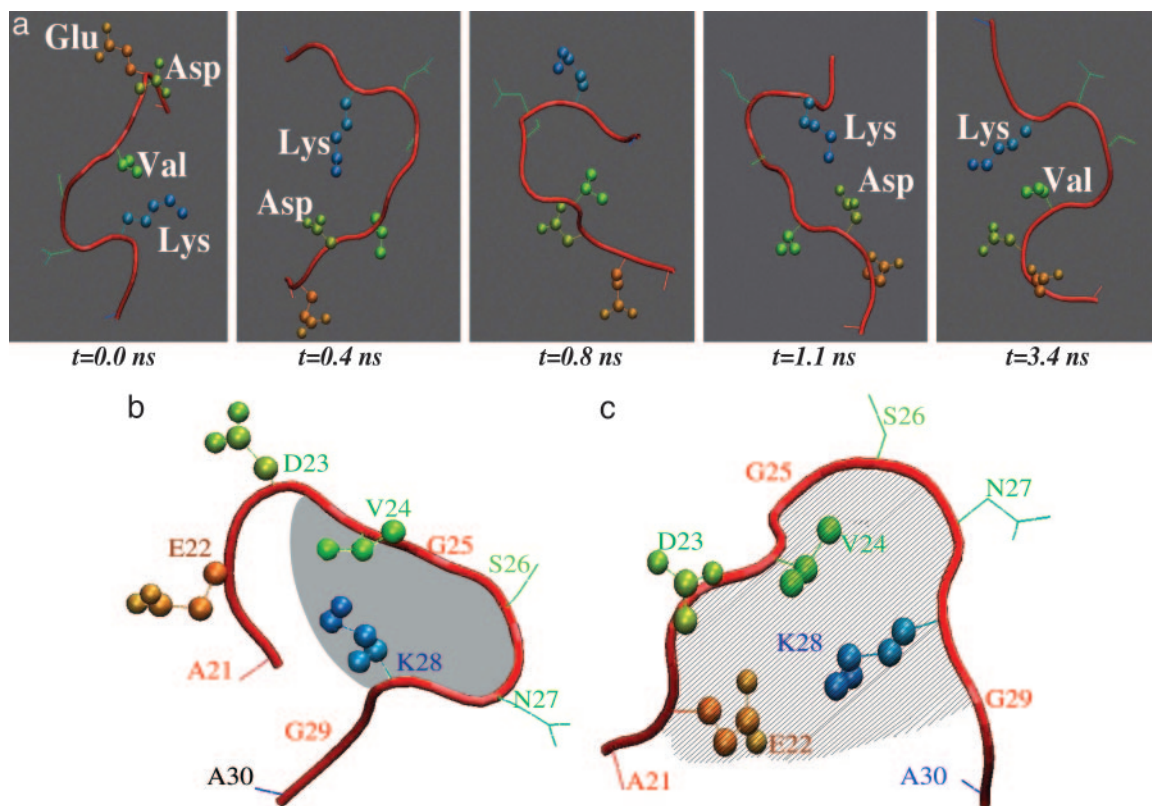| EI, kcal/mol	Glu-22–Lys-28			Asp-23–Lys-28		
	B	B^-	B^+	B	B^-	B^+
0.0	7	1	5	6	1	1
1.5	28	6	16	22	7	9
2.5	48	5	21	40	11	13

Fig. 3. Representative Aβ (21–30) conformations. (*a*) Series of alternate Val-24–Lys-28 unpacking/packing events due to formation of transient Asp-23–Lys-28 contact. (*b*) Representative loop conformation of class *B⁻*. Lys-28 side chain points opposite to the normal vector of the loop plane. (*c*) Representative conformation for class *B⁺*. Glu-22 is close to Lys-28 in this conformation. Lys-28 points along the normal vector to the loop plane.

fold, perturbations in loop stability could enhance or block fibril formation. A substitution of Glu-22 by a nonnegatively charged amino acid could enhance the model fibril formation through two different mechanisms: (*i*) decrease of loop stability and subsequent increase in the population of aggregation-prone unpacked conformations and (*ii*) increase in the rate of Asp-23–Lys-28 contact formation because Glu-22 no longer competes with Asp-23 for a stable interaction with Lys-28.

Summary

We employed discrete MD and a united-atom model to visualize the conformational dynamics of Aβ(21–30), a region of Aβ hypothesized to be the nucleation center of Aβ monomer folding. Simulations at equilibrium conditions reveal a stable loop structure in the central region (Val-24–Lys-28), which is stabilized by hydrophobic interactions, and a high degree of

flexibility in other areas. Correlation of perturbations of loop stability with changes in the electrostatic component of the force field provide an energy-based interpretation for the effects of familial AD mutations causing amino acid substitution at Glu-22. Our simulations are consistent with experimental studies of Aβ(21–30) and provide mechanistic insight into how conformational changes in the structure of the Aβ monomer may affect peptide self-assembly and aggregation.

1. Pike, C. J., Walencewicz1, A. J., Glabe, C. G. & Cotma, C. W. (1991) *Brain Res.* **563,** 311–314.
2. Walsh, D. M., Lomakin, A., Benedek, G. B., Condron, M. M. & Teplow, D. B. (1997) *J. Biol. Chem.* **272,** 22364–22372.
3. Harper, J. D., Wong, S. S., Lieber, C. M. & Lansbury, P. T. (1997) *Chem. Biol.* **4,** 119–125.
4. Lambert, M. P., Barlow, A. K., Chromy, B. A., Edwards, C., Freed, R., Liosatos, M, Morgan, T. E., Rozovsky, I., Trommer, B., Viola, K. L., *et al*. (1998) *Proc. Natl. Acad. Sci. USA* **95,** 6448–6453.
5. Yong, W., Lomakin, A., Kirkitadze, M. D., Teplow, D. B., Chen, S. H. & Benedek, G. B. (2002) *Proc. Natl. Acad. Sci. USA* **99,** 150–154.
6. Walsh, D. M., Klyubin, I., Fadeeva, J. V., Cullen, W. K., Anwyl, R., Wolfe, M. S., Rowan, M. J. & Selkoe, D. J. (2002) *Nature* **416,** 535–539.
7. Kayed, R., Head, E., Thompson, J. L., McIntire, T. M., Milton, S. C., Cotman, C. W. & Glabe, C. G. (2003) *Science* **300,** 486–489.
8. Nilsberth, C., Westlind-Danielsson, A., Eckman, C. B., Condron, M. M.,
Axelman, K., Forsell, C., Stenh, C., Luthman, J., Teplow, D. B., Younkin, S. G., *et al*. (2001) *Nat. Neurosci.* **4,** 887–893.
9. Klein, W. L., Stine, W. B. & Teplow, D. B. (2004) *Neurobiol. Aging* **25,** 569–580.
10. Lazo, N. D., Grant, M. A., Condron, M. C., Rigby, A. C. & Teplow, D. B. (2005) *Protein Sci.,* in press.
11. Zhou, Y. Q. & Karplus, M. (1997) *Proc. Natl. Acad. Sci. USA* **94,** 14429–14432.
12. Borreguero, J. M., Dokholyan, N. V., Buldyrev, S. V., Shakhnovich, E. I. & Stanley, H. E. (2002) *J. Mol. Biol.* **318,** 863–876.
13. Borreguero, J. M., Ding, F., Buldyrev, S. V., Stanley, H. E. & Dokholyany, N. V. (2004) *Biophys. J.* **87,** 521–533.
14. Ding, F., Dokholyan, N. V., Buldyrev, S. V., Stanley, H. E. & Shakhnovich, E. I. (2002) *Biophys. J.* **83,** 3525–3532.
15. Smith, A. V. & Hall, C. K. (2001) *J. Mol. Biol.* **312,** 187–202.
16. Peng, S., Ding, F., Urbanc, B., Buldyrev, S. V., Cruz, L., Stanley, H. E. & Dokholyan, N. V. (2004) *Phys. Rev. E Stat. Phys. Plasmas Fluids Relat. Interdiscip. Top.* **69,** 041908.

BIOPHYSICS

17. Urbanc, B., Cruz, L., Yun, S., Ding, F., Buldyrev, S. V., Bitan, G., Teplow, D. B. & Stanley, H. E. (2004) *Proc. Natl. Acad. Sci. USA* **101,** 17345–17350.
18. Ding, F., Buldyrev, S. V. & Dokholyan, N. V. (2004) *Biophys. J.* **88,** 147–155.
19. Eaton, W. A., Muñoz, V, Hagen, J. S. J., Jas, G. S., Lapidus, L. J., Henry, E. R. & Hofrichter, J. (2000) *Annu. Rev. Biophys. Biomol. Struct.* **29,** 327–359.
20. Onuchic, J. N., Nymeyer, H., García, A. E., Chahine, J. & Socci, J. N. (2000) *Adv. Protein Chem.* **53,** 87–152.
21. Sanner, M. F., Olson, A. J. & Spehner, J. (1996) *Biopolymers* **38,** 305–320.
22. Urbanc, B., Cruz, L., Ding, F., Sammond, D., Khare, S., Buldyrev, S. V., Stanley, H. E. & Dokholyan, N. V. (2004) *Biophys. J.* **87,** 2310–2321.
23. Pathria, R. K. (1996) *Statistical Mechanics* (Butterworth–Heinemann, Boston), 2nd Ed.
24. D'Ursi, A. M., Armenante, M. R., Guerrini, R., Salvadori, S., Sorrentino, G. & Picone, D. (2002) *J. Med. Chem.* **47,** 4231–4238.
25. Petkova, A. T., Ishii, Y., Balbach, J. J., Antzutkin, O. N., Leapman, R. D., Delaglio, F. & Tycko, R. (2002) *Proc. Natl. Acad. Sci. USA* **99,** 16742–16747.
26. Li, L., Darden, T. A., Bartolotti, L., Kominos, D. & Pedersen, L. G. (1999) *Biophys. J.* **76,** 2871–2878.
27. Ma, B. & Nussinov, R. (2002) *Proc. Natl. Acad. Sci. USA* **99,** 14126–14131.
28. Hutchinson, E. G. & Thornton, J. M. (1994) *Protein Sci.* **3,** 2207–2216.
29. Ramírez-Alvarado, M., Kortemme, T., Blanco, F. J. & Serrano, L. (1999) *Bioorg. Med. Chem.* **7,** 93–103.
30. Espinosa, J. F., Muñoz, V. & Gellman, S. H. (2001) *J. Mol. Biol.* **306,** 397–402.
31. Hou, L., Shao, H., Zhang, Y., Li, H., Menon, N. K., Neuhaus, E. B., Brewer, J. M., Byeon, I. L., Ray, D. G., Vitek, M. P., *et al.* (2004) *J. Am. Chem. Soc.* **126,** 1992–2005.
32. Horovitz, A. & Fersht, A. R. (1992) *J. Mol. Biol.* **224,** 733–740.
33. Searle, M. S., Griffiths-Jones, S. R. & Skinner-Smith, H. (1999) *J. Am. Chem. Soc.* **121,** 11615–11620.
34. Kumar, S. & Nussinov, R. (1999) *J. Mol. Biol.* **293,** 1241–1255.
35. Sciarretta, K. L., Gordon, D. J., Petkova, A. T., Tycko, R. & Meredith, S. C. (2005) *Biochemistry*, in press.
36. Nostrand, W. E. V., Melchor, J. P., Cho, H. S., Greenberg, S. M. & Rebeck, G. W. (2001) *J. Biol. Chem.* **276,** 32860–32866.